

**Microscopic coexistence of antiferromagnetic order and  
superconductivity in  $\text{Ba}_{0.77}\text{K}_{0.23}\text{Fe}_2\text{As}_2$**

Z. Li,<sup>1</sup> R. Zhou,<sup>1</sup> D. L. Sun,<sup>2</sup> J. Yang,<sup>1</sup> C. T. Lin,<sup>2</sup> and Guo-qing Zheng<sup>3,1</sup>

<sup>1</sup>*Institute of Physics and Beijing National Laboratory for Condensed Matter Physics,  
Chinese Academy of Sciences, Beijing 100190, China*

<sup>2</sup>*Max Planck Institute - Heisenbergstrasse 1, D-70569 Stuttgart, Germany*

<sup>3</sup>*Department of Physics, Okayama University, Okayama 700-8530, Japan*

(Dated: November 29, 2019)

The relationship between antiferromagnetism (AFM) and superconductivity (SC) is an important subject in condensed-matter physics. In heavy-fermion compounds, AFM and SC coexist microscopically [1–3]. The same is true in some cuprate high-temperature superconductors [4]. In the recently-discovered iron-pnictides [5], it is unclear whether AFM and SC can coexist or they compete one another [6–13]. Here we address the issue by  $^{75}\text{As}$  nuclear magnetic resonance (NMR) measurements on single-crystal  $\text{Ba}_{0.77}\text{K}_{0.23}\text{Fe}_2\text{As}_2$ . Below  $T_N=46$  K, we find that the NMR transition lines for  $H \parallel c$  split and those for  $H \parallel a$  shift, indicating that AFM sets in, with the ordered moment lying on the  $ab$ -plane. The spin lattice relaxation rate measured in the ordered state shows a distinct decrease below  $T_c(H=12\text{ T})=16$  K, following a  $T^3$  relation. Our results show unambiguously that the electrons hyperfine-coupled to  $^{75}\text{As}$ -nuclei are responsible for both AFM and SC. Furthermore, the ordered moment is unchanged below  $T_c$ , indicating that AFM and SC do not compete but coexist microscopically.

Figure 1 shows the phase diagram of  $\text{Ba}_{1-x}\text{K}_x\text{Fe}_2\text{As}_2$ . The red squares designate Neel temperature  $T_N$  determined by NMR spectra and  $T_1$  measurements and the open squares are adapted from ref.[14]. The black circles indicate the superconducting transition temperature  $T_c$  determined by susceptibility measurements. The samples with  $x=0.23$  and  $0.24$  belong to the underdoped regime.

Figure 2 shows the frequency-scanned  $^{75}\text{As}$  NMR spectra for  $\text{Ba}_{0.77}\text{K}_{0.23}\text{Fe}_2\text{As}_2$  with both  $H \parallel c$ -axis and  $H \parallel a$ -axis configurations. The spectrum at  $T = 100$  K in the paramagnetic state shows a sharp central peak accompanied by two satellite peaks due to nuclear quadrupole interaction. The nuclear quadrupole frequency  $\nu_Q$  is found to be 5.06 MHz which is a little smaller than the optimally doped sample (5.1 MHz) [15]. The spectra change below  $T_N=46$  K. Namely, all the three peaks split for  $H \parallel c$ , while the peaks shifted to higher frequencies for  $H \parallel a$ . In the antiferromagnetically ordered state, neutron experiments have found that the Fe magnetic moments lie on the  $ab$ -plane, forming stripes[16]. The internal magnetic field at the As site located above or below the magnetically-ordered Fe layer should direct along the  $c$ -axis or anti-parallel to the  $c$ -axis (see Supplementary Information). In such a case, for  $H \parallel c$ , the effective field seen by the As nuclei sitting above or below the Fe layer is  $H_c^{\text{eff}} = H_0 \pm H_{\text{int}}$ , which will split the spectra into two sets. One set consisting of the central transition and two satellites, which corresponds to the As sitting above the

Fe layer, shifted up by the amount of  $\gamma H_{\text{int}}$ , and the other set corresponding to the As sitting below the Fe layer shifted down by the same amount. For  $H \parallel a$ , on the other hand,  $H_{\text{a}}^{\text{eff}} = \sqrt{H_0^2 + H_{\text{int}}^2}$  will simply shift each peak to a higher resonance frequency [17]. The spectra shown in Fig. 2 show that the As nuclei indeed experience such internal magnetic fields below  $T_{\text{N}}=46$  K. The same is true for the  $x=0.24$  sample (data not shown).

As seen in Fig. 2 (a), for  $H \parallel c$ , the two sets of the spectra happen to overlap with each other, resulting in five peaks of which the central one being the broadest. The solid curve is the simulation of the summation of the two sets of the spectra. In the calculation, the area ratio of a satellite peak to the central peak is set to 3:4 according to the theoretical requirement which is indeed satisfied at  $T=100$  K. Such calculation fits the spectra very well below  $T=35$  K, indicating that the whole sample is in the antiferromagnetically ordered state below this temperature. However, in the temperature range between 35 K and  $T_{\text{N}}=46$  K, the agreement between the calculation and the observed spectra is poor; the height of the observed central peak is larger than calculated. This indicates that the transition into the antiferromagnetically ordered state is of first order. In fact, the splitting does not decrease continuously toward  $T_{\text{N}}$  as would be expected for a second-order phase transition.

The internal field  $H_{\text{int}}$  can be deduced from the shift of the central peak for  $H \parallel a$  and/or the splitting of the peaks for  $H \parallel c$ . The temperature dependence of  $H_{\text{int}}$  is shown in Fig. 3. Below  $T_{\text{N}}$  the internal field develops rapidly, reaching to 0.8 T at  $T=9$  K. The saturated internal field is about half that for undoped parent compound with  $T_{\text{N}} \sim 140$  K ( $H_{\text{int}} \sim 1.5$  T). For  $H \parallel c$ , the signal becomes very weak below  $T=25$  K, since the spectrum is spread over a wide frequency range. For  $H \parallel a$ , on the other hand, the uncertainty to calculate  $H_{\text{int}}$  from the peak shift becomes large near  $T_{\text{N}}$ .

The right axis of Fig. 3 is the magnitude of the ordered magnetic moment per Fe atom, which is deduced from the internal field by reasonably assuming that the hyperfine coupling constant is the same as in the undoped compound [17]. The estimated moment size at  $T=9$  K is about  $0.45 \mu_{\text{B}}$ , which is about half that in undoped compound [16].

Next we discuss the temperature dependence of the spin lattice relaxation rate  $1/T_1$  which is measured at the central peak for  $H \parallel a$  and plotted in Fig. 4. The  $1/T_1$  shows an upturn with decreasing  $T$  and forms a peak at  $T_{\text{N}}=46$  K, due to a critical slowing down of the magnetic moments. Below  $T_{\text{N}}=46$  K,  $1/T_1$  decreases and becomes to be in proportion to  $T$  before superconductivity sets in. Below  $T_{\text{c}}(H=12 \text{ T})=16$  K,  $1/T_1$  shows another sharp

reduction, and follows a  $T^3$  relation. At further low temperatures, the decrease of  $1/T_1$  becomes gradual.

It should be emphasized that below  $T_N=46$  K,  $1/T_1$  was measured at the shifted peak that experiences an internal magnetic field. Therefore, the sharp decrease of  $1/T_1$  below  $T_c$  indicates that the electrons hyperfine-coupled to the nuclei produce both the magnetic order and superconductivity. Our results are clear and most direct evidence that AFM coexists microscopically with superconductivity. Furthermore,  $H_{\text{int}}$  is unchanged below  $T_c$ , as can be seen in Fig. 3, which indicates that AFM and SC do not compete. Therefore, the microscopic coexistence of magnetism and superconductivity is a common rule rather than an exception, in view of what have been seen in heavy fermions and cuprates. Our results show that iron pnictides is a new member of this paradigm of coexisting states of matter.

In Ce-based heavy fermion compounds, the same electronic band derived from Ce-4f<sup>1</sup> electrons is responsible for both AFM and SC, so that the ordered magnetic moment is small [1, 2]. In such case, AFM and SC may be envisaged as different sides of a single coin [18]. In U-based heavy fermion compound UPd<sub>2</sub>Al<sub>3</sub> that is a multi-band system, on the other hand, the situation is more complex. It is believed that different electron bands bare respective responsibility for AFM and SC, which allows a large ordered magnetic moment of  $0.85 \mu_B$  to coexist with SC [3, 19]. The current compound is also a multi-band system, with some orbitals strongly Hund-coupled which are more localized and the others more itinerant due to stronger hybridization with As-2p orbitals [20]. It is plausible that the moderate size of the ordered moment arises from the more localized *d*-orbitals, so that it can coexist with SC which is mainly due to the more itinerant orbitals. Thus, our work demonstrates the richness of physics of multiple-orbital electron systems.

Finally, we note that the temperature dependence of  $1/T_1$  below  $T_c$  is much weaker than in the optimally-doped sample Ba<sub>0.68</sub>K<sub>0.32</sub>Fe<sub>2</sub>As<sub>2</sub> ( $T_c=38.5$  K) where  $1/T_1$  follows an exponential decrease down to very low temperatures [15]. Impurity scattering is difficult to explain the difference since both samples have similar degree of cleanness as evidenced by the similar NMR linewidth (83 kHz at  $T=100$  K and  $H=7$  T). We therefore attribute such weaker  $T$  dependence to the coexisting magnetism. Two existing theories may explain such behavior. One is the odd-frequency superconducting state proposed for heavy fermions near a quantum critical point which is a gapless state [21]. The other is a theory proposed for iron pnictides where a nodal superconducting gap is stabilized in the doping region coexisting

with magnetic order [22].

## Methods

The single crystals of  $\text{Ba}_{1-x}\text{K}_x\text{Fe}_2\text{As}_2$  with  $0.23 \leq x \leq 1$  were grown by using the self-flux method and the K-content was determined by Inductively-Coupled-Plasma method [23]. The samples with  $x=0.23, 0.24, 0.32$  [15] and 0.61 were selected for NMR measurements. Each sample has a typical surface size of  $4 \text{ mm} \times 1.5 \text{ mm}$ . The  $T_c$  was measured by both DC susceptibility using a superconducting quantum interference device and by AC susceptibility using an in-situ NMR coil at zero field and at  $H=12 \text{ T}$ . For the  $x=0.23$  sample ( $T_c=16.5 \text{ K}$ ),  $T_c$  decreases to 16 K for  $H_0(= 12 \text{ T}) \parallel a$  axis and to 15.5 K for  $H_0(= 12 \text{ T}) \parallel c$  axis. The spectra of  $^{75}\text{As}$  with the nuclear gyromagnetic ratio  $\gamma = 7.2919 \text{ MHz/T}$  are obtained by scanning the RF frequency at a fixed magnetic field  $H_0(= 11.9977 \text{ T})$ . The  $1/T_1$  was determined from an excellent fit of the nuclear magnetization to  $1 - M(t)/M(\infty) = 0.1\exp(-t/T_1) + 0.9\exp(-6t/T_1)$  for the central transition peak, where  $M(t)$  is the nuclear magnetization at time  $t$  after the saturation pulse [24]. The quantity  $1/T_1T$  shows a systematic doping dependence (see Supplementary Information) .

- 
- [1] Kawasaki, S. *et al.* Gapless magnetic and quasiparticle excitations due to the coexistence of antiferromagnetism and superconductivity in  $\text{CeRhIn}_5$ : A study of  $^{115}\text{In}$  NQR under pressure. *Phys. Rev. Lett.* **91**, 137001 (2003).
  - [2] Zheng, G.Q. *et al.* Coexistence of antiferromagnetic order and unconventional superconductivity in heavy-fermion  $\text{CeRh}_{1-x}\text{Ir}_x\text{In}_5$  compounds: Nuclear quadrupole resonance studies. *Phys. Rev. B* **70**, 014511 (2004).
  - [3] Sato, N.K. *et al.* Strong coupling between local moments and superconducting 'heavy' electrons in  $\text{UPd}_2\text{Al}_3$ . *Nature* **410**, 340-343 (2001).
  - [4] Mukuda, H., Shimizu, S., Iyo, A. & Kitaoka, Y. High-T(c) Superconductivity and Antiferromagnetism in Multilayered Copper Oxides -A New Paradigm of Superconducting Mechanism-. *J. Phys. Soc. Jpn.* **81**, 011008 (2012).
  - [5] Kamihara, Y., Watanabe, T., Hirano, M. & Hosono, H. Iron-based layered superconductor  $\text{La}[\text{O}_{1-x}\text{F}_x]\text{FeAs}$  ( $x=0.05-0.12$ ) with  $T_c=26 \text{ K}$ . *J. Am. Chem. Soc.* **130**, 3296 (2008).
  - [6] Chen, H. *et al.* Coexistence of the spin-density wave and superconductivity in  $\text{Ba}_{1-x}\text{K}_x\text{Fe}_2\text{As}_2$ .

- Europhys. Lett. **85**, 17006 (2009).
- [7] Julien, M.H. *et al.* Homogeneous vs. inhomogeneous coexistence of magnetic order and superconductivity probed by NMR in Co- and K-doped iron pnictides. Europhys. Lett. **87**, 37001 (2009).
- [8] Park, J.T. *et al.* Electronic Phase Separation in the Slightly Underdoped Iron Pnictide Superconductor  $\text{Ba}_{1-x}\text{K}_x\text{Fe}_2\text{As}_2$ . Phys. Rev. Lett. **102**, 117006 (2009).
- [9] Wiesenmayer, E. *et al.* Microscopic Coexistence of Superconductivity and Magnetism in  $\text{Ba}_{1-x}\text{K}_x\text{Fe}_2\text{As}_2$ . Phys. Rev. Lett. **107**, 237001 (2011).
- [10] Iye, T. *et al.* Microscopic Evidence of Direct Coupling between Magnetic and Superconducting Order Parameters in  $\text{BaFe}_2(\text{As}_{1-x}\text{P}_x)_2$ . J. Phys. Soc. Jpn. **81**, 033701 (2012).
- [11] Baek, S.H. *et al.* NMR Investigation of Superconductivity and Antiferromagnetism in  $\text{CaFe}_2\text{As}_2$  under Pressure. Phys. Rev. Lett. **102**, 227601 (2009).
- [12] Laplace, Y., Bobroff, J., Rullier-Albenque, F., Colson, D. & Forget, A. Atomic coexistence of superconductivity and incommensurate magnetic order in the pnictide  $\text{Ba}(\text{Fe}_{1-x}\text{Co}_x)_2\text{As}_2$ . Phys. Rev. B **80**, 140501 (2009).
- [13] Urbano, R.R. *et al.* Distinct High-T Transitions in Underdoped  $\text{Ba}_{1-x}\text{K}_x\text{Fe}_2\text{As}_2$ . Phys. Rev. Lett. **105**, 107001 (2010).
- [14] Rotter, M., Pangerl, M., Tegel, M. & Johrendt, D. Superconductivity and Crystal Structures of  $(\text{Ba}_{1-x}\text{K}_x)\text{Fe}_2\text{As}_2$  ( $x=0-1$ ). Angew. Chem. Int. Ed. **47**, 7949-7952 (2008).
- [15] Li, Z. *et al.* Nodeless energy gaps of single-crystalline  $\text{Ba}_{0.68}\text{K}_{0.32}\text{Fe}_2\text{As}_2$  as seen via  $(75)\text{As}$  NMR. Phys. Rev. B **83**, 140506 (2011).
- [16] Huang, Q. *et al.* Neutron-Diffraction Measurements of Magnetic Order and a Structural Transition in the Parent  $\text{BaFe}_2\text{As}_2$  Compound of FeAs-Based High-Temperature Superconductors. Phys. Rev. Lett. **101**, 257003 (2008).
- [17] Kitagawa, K., Katayama, N., Ohgushi, K., Yoshida, M. & Takigawa, M. Commensurate Itinerant Antiferromagnetism in  $\text{BaFe}_2\text{As}_2$ :  $^{75}\text{As}$ -NMR Studies on a Self-Flux Grown Single Crystal. J. Phys. Soc. Jpn. **77**, 114709 (2008).
- [18] Zhang, S.C., A unified theory based on  $\text{SO}(5)$  symmetry of superconductivity and antiferromagnetism, Science **275**, 1089 (1997).
- [19] Yotsuhashi, S., Kusunose, H. & Miyake, K., Orbital dependence in Kondo effect enlarged by Hund's rule coupling. J. Phys. Soc. Jpn **70**, 186-191 (2001).

- [20] Lu, Ma, F., Lu, Z.Y. & Xiang, T., Electronic structure of ternary iron arsenides  $A\text{Fe}_2\text{As}_2$  (A=Ba, Ca, or Sr), *Front. Phys. China*, **5**, 150-160 (2010).
- [21] Fuseya, Y., Kohno, H. & Miyake, K. Realization of odd-frequency p-wave spin-singlet superconductivity coexisting with antiferromagnetic order near quantum critical point. *J. Phys. Soc. Jpn.* **72**, 2914-2923 (2003).
- [22] Maiti, S., Fernandes, R.M. & Chubukov, A.V. Gap nodes induced by coexistence with antiferromagnetism in iron-based superconductors.pdf. *arXiv* **1203**, 0991 (2012).
- [23] Sun, G.L. *et al.* Single Crystal Growth and Effect of Doping on Structural, Transport and Magnetic Properties of  $A_{1-x}K_x\text{Fe}_2\text{As}_2$  (A = Ba, Sr). *J. Supercond. Nov. Magn.* **24**, 1773-1785 (2011).
- [24] Narath, A. Nuclear Spin-Lattice Relaxation in Hexagonal Transition Metals: Titanium. *Phys. Rev.* **162**, 320-332 (1967).

**Acknowledgements** We thank K. Miyake and T. Xiang for useful discussions and comments.

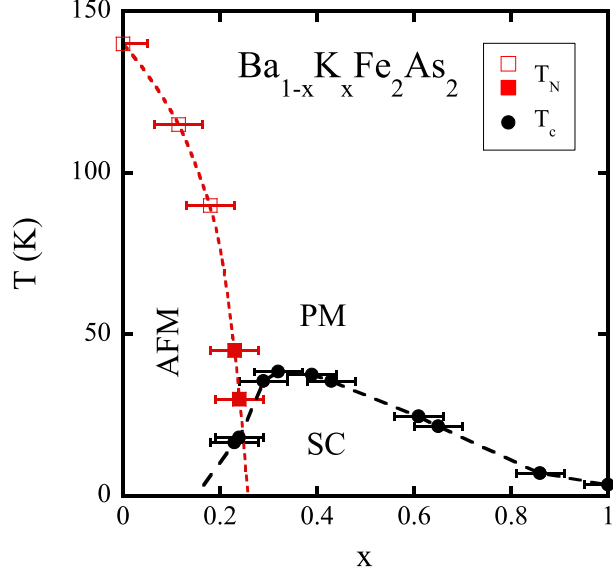


FIG. 1: Phase diagram of  $\text{Ba}_{1-x}\text{K}_x\text{Fe}_2\text{As}_2$ . The red squares designate the Neel temperature  $T_N$  determined from NMR measurements and the open squares are adapted from ref.[14]. The black circles indicate superconducting transition temperatures determined from susceptibility measurements. AFM, PM and SC represent antiferromagnetically ordered, paramagnetic and superconducting states, respectively.

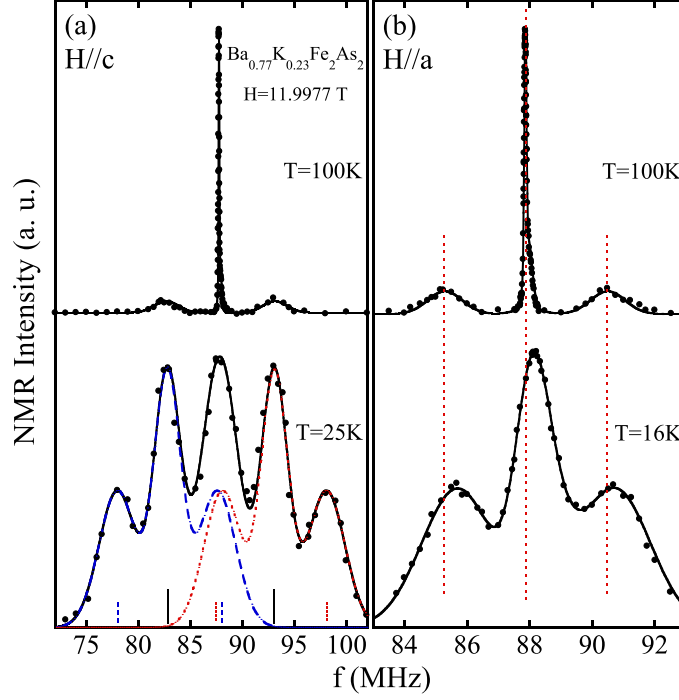


FIG. 2:  $^{75}\text{As}$  NMR spectra above and below  $T_N$  for (a)  $H \parallel c$  and (b)  $H \parallel a$  respectively. The vertical axis for the  $T = 100$  K spectra was offset for clarity. (a) The blue dash curve and the red dot curve are the simulated two sets of spectra that are split by the internal magnetic field, and the black curve is the sum of the two sets of spectra. The short lines designate peak positions. (b) The straight dash lines designate peak positions of the  $T = 100$  K spectrum.

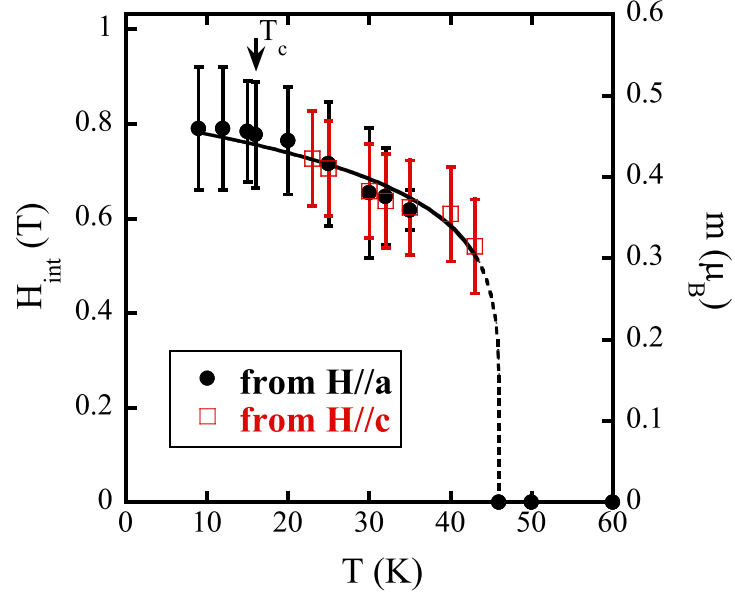


FIG. 3:  $T$  dependence of the internal magnetic field  $H_{\text{int}}$  (left axis) and the ordered magnetic moment (right axis). The black circles and open squares are deduced from the spectra with  $H \parallel a$  and  $H \parallel c$ , respectively. The curve is a guide to the eyes.

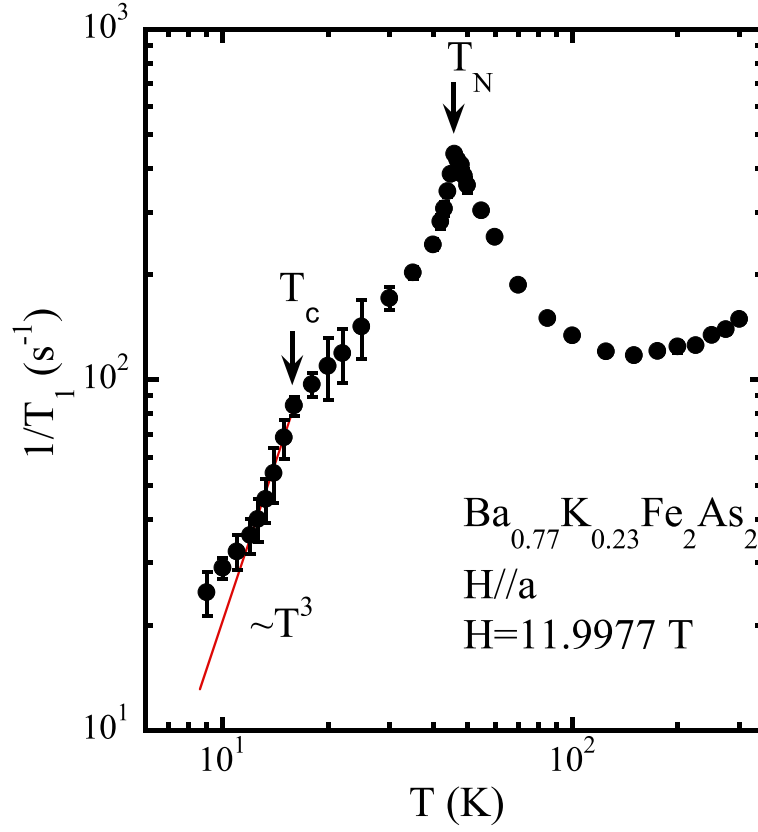


FIG. 4: The temperature dependence of the spin-lattice relaxation rate  $1/T_1$ . The red line indicates the  $1/T_1 \propto T^3$  relation.

Supplementary Information for **Microscopic coexistence of antiferromagnetic order and superconductivity in  $\text{Ba}_{0.77}\text{K}_{0.23}\text{Fe}_2\text{As}_2$**

Figure 5 (a) and (b) shows the effective magnetic field at the As-sites, with the external field applied along the  $c$ -axis and along the  $a$ -axis, respectively.

In Fig. 6, we show the quantity  $1/T_1T$  as a function of temperature for the underdoped ( $x=0.23$ ), optimally-doped ( $x=0.32$ ,  $T_c=38.5$  K) and overdoped ( $x=0.61$ ,  $T_c=24.5$  K) samples. None of them shows a Korringa relation ( $1/T_1T = \text{const.}$ ) expected for a conventional metal. The  $1/T_1T$  increases with decreasing temperature for underdoped and optimally-doped sample, which is due to the antiferromagnetic spin fluctuations. At high temperatures, the value of  $1/T_1T$  which is dominated by the density of states (DOS) at the Fermi level, increases with increasing  $x$ , which indicates that the DOS increases with increasing doping.

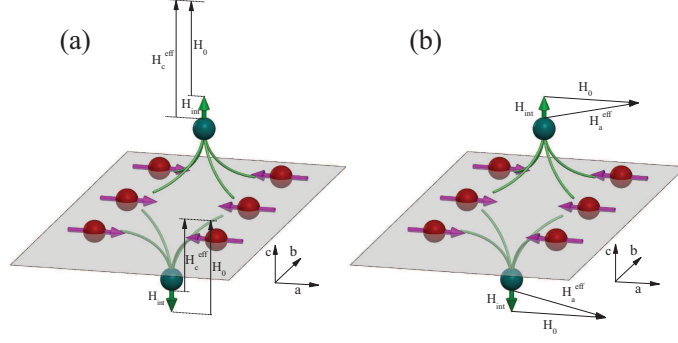


FIG. 5: **Supplementary Material** The effective magnetic field at the As-sites, when the external field is applied along the  $c$ -axis (a) and along the  $a$ -axis (b), respectively.

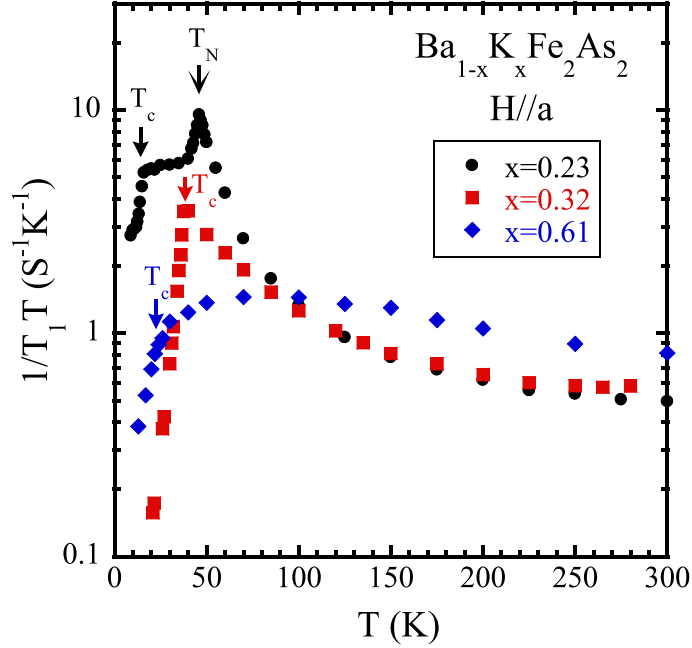


FIG. 6: **Supplementary Material** The  $T$  dependence of  $1/T_1 T$  of  $\text{Ba}_{1-x}\text{K}_x\text{Fe}_2\text{As}_2$  with  $x=0.23$ , 0.32 and 0.61.